JGR Oceans

RESEARCH ARTICLE
10.1029/2022JC019608

Upper Ocean Transport in the Anegada Passage From Multi-Year Glider Surveys

J. C. Gradone[1], W. D. Wilson[2,3], S. M. Glenn[1], and T. N. Miles[1]

[1]Center for Ocean Observing Leadership, Department of Marine and Coastal Sciences, School of Environmental and Biological Sciences, Rutgers University, New Brunswick, NJ, USA, [2]Center for Marine and Environmental Studies, University of the Virgin Islands, St. Thomas, VI, USA, [3]Ocean and Coastal Observing—Virgin Islands, Inc, St. Thomas, VI, USA

Key Points:

- Total transport and transport of South Atlantic Water through the Anegada Passage (AP) may be larger than previously estimated
- The AP is a pathway for both Atlantic Meridional Overturning Circulation return flow and subtropical gyre recirculation
- Gliders are an effective component of the global ocean observing system, needed for measuring subsurface water mass structure and transport

Correspondence to:
J. C. Gradone,
jgradone@marine.rutgers.edu

Citation:
Gradone, J. C., Wilson, W. D., Glenn, S. M., & Miles, T. N. (2023). Upper ocean transport in the Anegada Passage from multi-year glider surveys. *Journal of Geophysical Research: Oceans*, *128*, e2022JC019608. https://doi.org/10.1029/2022JC019608

Received 22 DEC 2022
Accepted 6 JUL 2023

Abstract Caribbean through-flow accounts for two-thirds of the Florida Current and consequently is an important conduit of heat and salt fluxes in the upper limb of the Atlantic Meridional Overturning Circulation (AMOC). Considering there is evidence that up to one-half of the Florida Current originates as South Atlantic Water (SAW), determining the distribution of SAW throughout the Caribbean Island passages is important as this constitutes the major pathway for cross-equatorial AMOC return flow. The Anegada Passage (AP) is a major pathway for subtropical gyre inflow and suggested to be a potential SAW inflow pathway worth revisiting. Here, we present glider-based observations of temperature, salinity and subsurface velocity that represent the first observations of any type in the AP in nearly 20 years. An isopycnal water mass analysis is conducted to quantify the transport of water masses with South Atlantic or North Atlantic origin. Two potentially new aspects of AP transport are revealed. The total AP transport (−4.8 Sv) is shown to be larger than previously estimated, potentially by up to a factor of two. The transport of SAW through the AP (−1.66 Sv) is also shown to be larger than previously estimated, which represents 35% of the total transport reported here and 28% of the SAW entering the Caribbean north of the Windward Island Passages. These results indicate the AP may be an important pathway for cross-equatorial AMOC return flow. These results also provide evidence that gliders with acoustic doppler profilers are a viable method for measuring island passage transport.

Plain Language Summary The Caribbean Sea through-flow is a major transport pathway for heat and salt in the upper limb of the Atlantic Meridional Overturning Circulation (AMOC). The presence of water masses (bodies of water with distinct temperature and salinity properties) that originated in the South Atlantic (SAW) in the Northern Hemisphere is indicative of cross-equatorial AMOC return flow. Ship-based observations in the 1990's identified major pathways for this AMOC return flow but there is still a substantial amount of SAW that is taking an unknown, alternate route northward. This study presents the first observations in nearly 20 years of temperature, salinity, and subsurface velocity in the Anegada Passage (AP). Here, we perform a water mass analysis that suggests the total transport and SAW transport through the AP is larger than previously estimated. This result is significant as the AP may be an important pathway for AMOC return flow. This study also shows that autonomous underwater gliders are a viable method for measuring island passage transport.

1. Introduction

To maintain Earth's radiative balance, both the atmosphere and the ocean drive a net poleward heat flux. However, the net heat flux in the Atlantic Ocean is northward, even in the southern hemisphere. The Atlantic Meridional Overturning Circulation (AMOC) is responsible for this heat flux as warm surface waters are carried northward which is ultimately balanced by cold deep waters returning southward. Increases in anthropogenic atmospheric carbon dioxide (CO_2) leading to a greenhouse warming effect are expected to impact the AMOC in several ways. A reduction in the heat loss from the ocean to the atmosphere and an increase in the input of freshwater at higher latitudes are expected to lower water mass density in the deep-water formation regions (Gregory et al., 2005). Currently, there is evidence for and uncertainty around a slowdown in the AMOC (Caesar et al., 2018; Praetorius, 2018; Thornalley et al., 2018). It is vital to better understand the dynamics of this circulation as variations in the strength of the AMOC have been linked with significant changes in global climate (dos Santos et al., 2010; Schmidt et al., 2004). These AMOC variations have induced changes in global temperature, wind fields, and the hydrologic cycle (Rahmstorf, 2002).

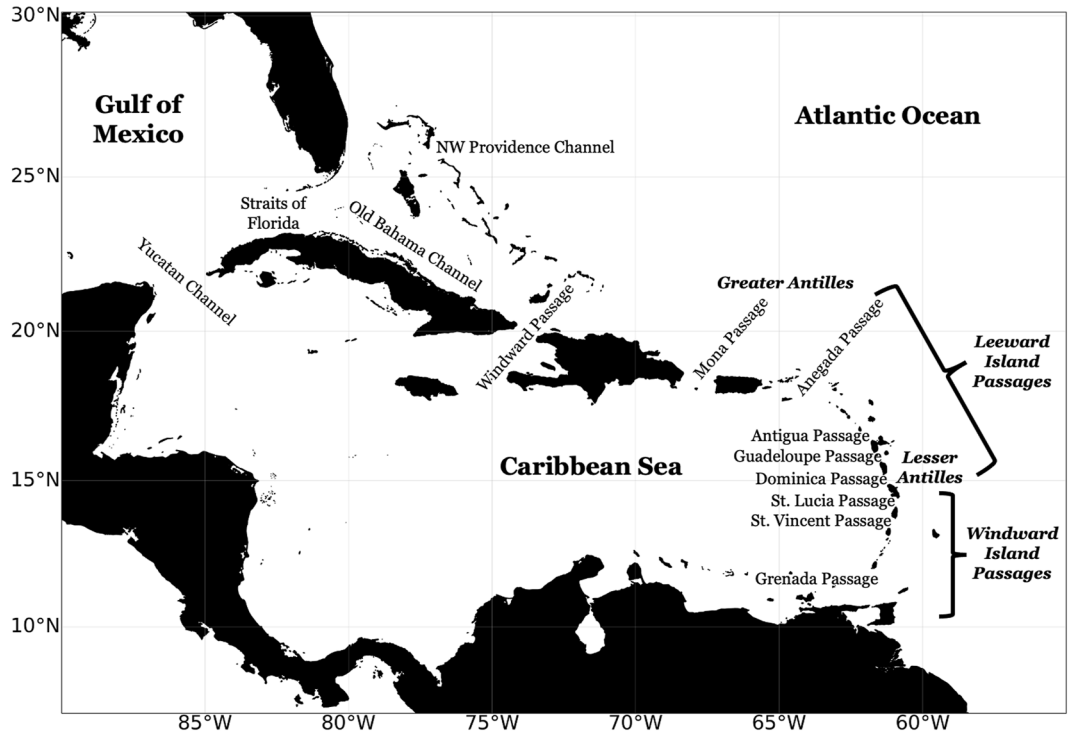

Figure 1. The Caribbean Sea with the major passages between the Atlantic Ocean and Caribbean Sea labeled.

Toward the beginning of the upper-limb of the AMOC's crossing into the North Atlantic lies the complex Caribbean Sea. This semi-enclosed basin is connected to the tropical Atlantic Ocean through a series of passages between the islands of the Greater and Lesser Antilles (Figure 1). The complex bathymetry of the eastern Caribbean passages effectively acts as a sieve for the inflow of Atlantic water due to the average sill depth being approximately 800 m (Johns et al., 2002). The inflow through these passages is highly dynamic. There is variability on synoptic, seasonal, annual, and decadal timescales and forcing from both winds and thermohaline circulation (Johns et al., 1999). Previous studies have found the net inflow to the Caribbean Sea of 28 Sv (1 Sverdrup = 10^6 m^3 s^{-1}) to be nearly equally geographically distributed in thirds: ∼10 Sv through the Greater Antilles passages, ∼8 Sv through the Leeward Island Passages, and ∼10 Sv through the Windward Island Passages (Johns et al., 2002). Throughout the remainder of this analysis, we discuss transport in units of Sverdrups, referring to transport into the Caribbean with a negative sign convention or using the term "inflow." Through a series of modeling experiments Johns et al. (2002) determined that the ∼10 Sv inflow through the Windward Island Passages to the south is almost entirely thermohaline forced as the wind-driven component is essentially zero. The ∼18 Sv inflow through the Greater Antilles and Leeward Islands Passages to the north was found to be driven by the large-scale subtropical gyre circulation. This inflow directly feeds into the dominant surface current, the Caribbean Current, which can account for up to two-thirds of the flow into the Gulf Stream at the Straits of Florida and consequently is an important conduit of mass, heat, salt, and freshwater fluxes in the AMOC (Johns et al., 2002).

While high-latitude sinking and interior mixing processes have a first order control on the magnitude of the AMOC, low-latitude wind-driven processes determine and modify the subsurface density structure of the water masses flowing through the Caribbean Sea, Gulf of Mexico, and eventually the Gulf Stream (Fratantoni et al., 2000). This linkage between upper ocean water mass conditions in the Caribbean and Gulf Stream activity is significant enough to be identifiable in paleoceanographic sediment core records. Planktonic foraminifera assemblages have linked high sea surface temperatures in the Caribbean with diminished Gulf Stream activity (Fischel et al., 2017; Reißig et al., 2019). This connection suggests that the inter-hemispheric atmospheric energy balance ultimately controls the large-scale circulation in this region through its influence on the position of the Intertropical Convergence Zone, which constitutes the main forcing for the North Atlantic Subtropical Gyre (STG) variability (Fischel et al., 2017; Nürnberg et al., 2021; Reißig et al., 2019).

In addition to forcing from STG variability, the modification of the subsurface density structure of the water masses flowing through the Caribbean Sea is also substantially impacted by upstream water mass origin. Historically, 45% (13 Sv) of the Florida Current transport has been considered to be of South Atlantic origin (Schmitz & Richardson, 1991; hereafter SR91), thus there is considerable interest in determining the distribution of South Atlantic Water (SAW) throughout the Caribbean Passages as this constitutes a major pathway for cross-equatorial AMOC return flow (Johns et al., 2002; Kirchner et al., 2009; Tuchen et al., 2022; Wilson & Johns, 1997). However, there are several significant inconsistencies recent publications have raised with the assumptions made by SR91 (Szuts & Meinen, 2017; hereafter SM17):

1. The accepted AMOC value at the time of the SR91's analysis was 13 Sv, whereas recent literature finds a mean value closer to 17 Sv in the Florida Straits at 26°N (Frajka-Williams et al., 2019; Szuts & Meinen, 2017).
2. SR91 consider the transport of all surface waters >24°C to be of South Atlantic origin in their formulation of a 13 Sv AMOC, whereas recent literature has found that surface waters that flow through the Florida Straits do not leave the subtropical gyre and thus potentially do not contribute to the strength of the AMOC (Brambilla & Talley, 2006).
3. SR91 ignore strong mid-depth horizontal gradients in eastern and western Salinity Max Waters and Central Waters in the Florida Current, which suggests these waters are not entirely North Atlantic Water (NAW) as SR91 assume.

In addition to the results from these recent publications, water mass analysis and transport estimates have shown a maximum of 11 ± 2.22 Sv of SAW flows in through the Windward Island Passages and approximately 5.3 ± 0.7 Sv of SAW flows northward from Guadeloupe to the Atlantic across 16°N (Rhein et al., 2005). When these SAW transport estimates are combined, a total SAW inflow of 16.3 Sv is in much better agreement with the accepted AMOC strength of 17 Sv. Therefore, we frame this analysis with an AMOC strength of 17 Sv but continue to reference the pioneering work by SR91 throughout the discussion while acknowledging both the limitations of several of their assumptions as well as the new understandings from more recent literature. With the pathway for a maximum of 11 Sv of SAW constrained to the Windward Island Passages, the route the remaining 6 Sv of SAW take northwards remains largely unresolved. There are uncertainties and consequences for projected changes in the AMOC (Frajka-Williams et al., 2019) and recent evidence that the Caribbean Sea is warming (Antuña-Marrero et al., 2015; Glenn et al., 2015; Jury, 2017), surface waters are freshening (Jury & Gouirand, 2011), and the through-flow is slowing (Jury, 2020). These factors combined with the lack of recent coordinated, sustained ocean observations in this region motivate a reassessment of transport through the Caribbean Passages.

The Anegada Passage (AP), located in the northeast corner of the Caribbean, is the largest and deepest of the Caribbean Passages (sill depth 1915 m, (Fratantoni et al., 1997)). Anegada Passage transport has been shown to be a major pathway for STG inflow in the form of NAW (Johns et al., 2002) and suggested to be an alternate pathway for SAW into the Caribbean (Johns et al., 1999; Wajsowicz, 2002; Wilson & Johns, 1997). Flow through the AP is predominately southwestward into the Caribbean where velocity profiles have shown a subsurface velocity maximum in the center of the passage and weak flow reversals found at times at the surface along both the eastern and western sides of the passage (Johns et al., 1999). There can also be strong eastward components over the western half of the passage and westward components over the eastern half of the passage, leading to strongly convergent flow (Johns et al., 1999).

The eastern Caribbean has been a historically under-sampled region until recently. Ship-based campaigns to collect direct transport observations throughout the Caribbean Passages during the 1990's and early 2000's (Johns et al., 1999, 2002; Kirchner et al., 2009; Rhein et al., 2005; Wilson & Johns, 1997) progressed the state of knowledge immensely. However, ship-based sampling is extremely expensive and limited by weather conditions. The development of autonomous underwater vehicles (gliders) has contributed to filling this data gap in the Caribbean Sea and other regions by providing high quality observations in a novel yet economical manner. Since 2020, gliders equipped with acoustic Doppler profilers (ADP) have been deployed throughout the AP region four separate times covering over ~2,700 km over ~150 days (Figure 2). While ADPs have been integrated onto gliders for over a decade (Miles et al., 2015; Todd et al., 2011, 2017), these field campaigns have served as a unique proof-of-concept that glider deployments can consistently observe passage transport variability at the same, if not better, quality and at comparatively lower cost than traditional ship-based campaigns (Schofield et al., 2007).

The present work builds upon previous Caribbean Passage transport research in several ways. Four glider deployments are utilized to both validate the methodology of using gliders to measure passage transport as well as develop further understandings of the transport dynamics in this region. In 2021, two glider deployments

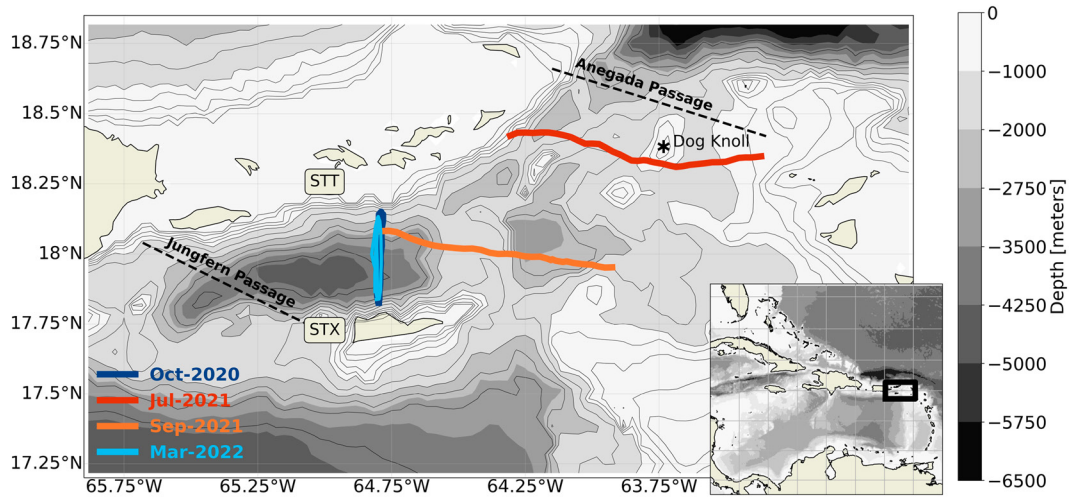

Figure 2. Glider tracks in the Anegada Passage region from 2020 to 2022 glider deployments.

ventured eastward across the AP on a path intentionally similar to historical ship-based transects to allow for a more direct comparison (Johns et al., 1999). In 2020 and 2022, single glider deployments were conducted on a repeating transect line between St. Thomas (STT) and St. Croix (STX) (15 transects in 2020, 6 transects in 2022) to allow for the calculation of a transport time-series from which additional details of the transport dynamics could be gathered. The high resolution, co-located glider observations of temperature, salinity, and subsurface velocity also allow for a detailed isopycnal water mass analysis to quantify the transport of water masses with South Atlantic or North Atlantic origin in the AP transport. To our best knowledge, the results presented in this study are the first published, detailed in-situ analysis of transport below 200 m in the AP region.

2. Observations and Methods

2.1. Transport From Glider-Mounted Acoustic Current Profiler Derived Horizontal Water Velocity

The observations used in this study were collected using Teledyne Webb Research Slocum gliders (Schofield et al., 2007). Gliders are buoyancy-driven, autonomous underwater vehicles that use a combination of changes in their pitch angle and internal volume to move vertically and horizontally in a sawtooth-like pattern. Gliders are modular platforms that can be instrumented with a growing variety of complex sensors. Two deep (1,000 m rated) Slocum gliders, RU29 and RU36, were used in this study. RU29 is a second-generation Slocum glider (G2) equipped with a Sea-Bird Scientific pumped conductivity, temperature, and depth (CTD) sensor and a 1-MHz Nortek AD2CP. RU36 is a third generation Slocum glider (G3) equipped with an RBR *legato*^{3} inductive cell CTD sensor, a 600-kHz Teledyne RD Instruments (TRDI) Pathfinder ADP, and an Aanderaa Oxygen Optode 4831. The Nortek AD2CP is a four-beam system that was configured to sample 8 pings per second in beam coordinates with a 0.2-m blanking distance in 0.5-m bins. The TRDI Pathfinder is also a four-beam system that was configured to sample one 10-ping ensemble average every second in beam coordinates with a 0.8-m blanking distance in 1-m bins. These configurations were chosen for a variety of reasons. Both instruments were configured to sample as quickly as possible, whereas the other configuration choices were a combination of power consumption capabilities and optimization testing. Data from both current profilers were logged internally and downloaded after the deployment. A summary of glider deployment details and specific configurations is provided in Table 1.

While two different types of current profilers were used in this study, measurements of water velocity relative to the glider were obtained using similar system configurations and processing techniques. The major data processing steps for both current profilers are quality control, correcting the beam velocities to level true-depth, mapping the beam velocities to vertical bins relative to the glider, performing a coordinate transformation to convert from beam to East-North-Up (ENU), and derivation of absolute horizontal water velocities. Raw beam velocity data are quality controlled first through several data screening filters. For the Nortek AD2CP, data below a correlation of 50% or above a high return amplitude of 75 dB are discarded (Todd et al., 2017). For the TRDI Pathfinder, data below a correlation threshold of 50%, an echo intensity of 70 dB, and percent good of 80% are discarded (Haines

Table 1
Glider Deployment Information, Configurations, and Summary of Transport Results

Deployment	October-2020	July-2021	September-2021	March-2022
Duration (days)	24	5.5	4.5	11
Location	St. Thomas-St. Croix	Outer AP	Outer AP	St. Thomas-St. Croix
Number of Transects	15	1	1	6
Current Profiler	Nortek AD2CP	Nortek AD2CP	Nortek AD2CP	TRDI Pathfinder
Absolute Transport from ADP Inversion Method	−2.27 ± 0.66 Sv	−4.43 Sv	−5.24 Sv	−2.47 ± 0.8 Sv
Geostrophic Transport from Thermal Wind	−2.29 ± 0.7 Sv	−4.74 Sv	−4.97 Sv	−3.49 ± 0.35 Sv
SAW Transport	−0.70 Sv	−1.21 Sv	−1.33 Sv	−0.84 Sv

et al., 2011; Taylor & Jonas, 2008). For both current profilers, glider pitch and roll as well as individual beam angles and directions are used to map beam velocity data to depth cells and then transformed to level true depth.

The Nortek AD2CP is mounted in a Janus configuration with beams 1 and 3 oriented forward and aft and slanted 47.5° off vertical and beams 2 and 4 oriented port and starboard and slanted 25° off vertical. A typical dive angle for Slocum gliders is 24–27° so either the forward or aft beams will be nearly horizontal on a climb or a dive for the Nortek system. Because of this configuration, only 3 beams are used in the transformation from beam to ENU velocity (beams 1, 2, and 4 on a dive and beams 2,3 and 4 on a climb). The TRDI Pathfinder is a phased array system also mounted in a Janus configuration where the four beams are angled 30° off vertical but rotated along the central axis of the glider so that beams 1 and 3 are oriented forward and beams 4 and 2 are oriented aft but 22.5° off the central axis of the glider to the port and starboard, respectively. Because of this configuration, all four beams can be used in the transformation from beam to ENU velocity. For both systems, an instrument specific transformation matrix based on the transducer face geometry is used to convert from beam to XYZ velocity (i.e., velocity relative to the glider). Next, another transformation matrix that incorporates the glider magnetic heading is used to convert from XYZ velocity to ENU (i.e., East-North-Up). A final round of quality control is then applied to the ENU velocity. Following Todd et al. (2017), velocities relative to the glider exceeding 75 cm s^{-1} are excluded as the glider's speed through water is ∼25 cm s^{-1} and larger relative velocities are not expected over the sampling range of the current profilers (maximum 20 m). Data from the velocity bin closest to the glider are also excluded as this bin can exhibit ringing or other frequent contamination. Lastly, data shallower than 5 m are discarded as the glider typically must travel several body lengths before it achieves a dive angle that is more closely representative of its typical flight behavior as compared to when it is on the surface.

Measurements made by glider-mounted current profilers combine the true water velocity, the velocity of the glider's motion, and noise:

$$U_{\text{adcp}} = U_{\text{ocean}} + U_{\text{glider}} + U_{\text{noise}} \quad (1)$$

There are several methods that can be used to derive absolute horizontal water velocities (U_{ocean}). Fundamentally, they either decompose the different components measured by glider-mounted current profilers or rely on assumptions to ignore them. The inversion method was originally developed for ship-based lowered current profilers (Visbeck, 2002) but has been adapted for use on gliders and used extensively (Ellis et al., 2015; Gradone et al., 2021; Heiderich & Todd, 2020; Ma et al., 2019; Miles et al., 2015; Todd et al., 2011, 2017). This method solves a system of equations for both unknown glider velocities and absolute horizontal water velocities using least squares techniques. An advantage of this method is that constraints (glider estimated depth-average currents, surface drift, bottom-track, etc.) can easily be applied to yield better estimates of the true horizontal water velocities. Additional constraints such as a curvature-minimizing smoothness constraint assist in reducing the noise from missing data (Visbeck, 2002). These constraints can be applied with different weights to determine the degree to which individual constraints should be considered. We follow Todd et al. (2011) by applying weights of 5 and 1 to our glider dead-reckoned depth-average current (DAC) and curvature-minimizing smoothness constraints, respectively. Figure 3 shows example DAC vectors from transects between St. Thomas and St. Croix during the October 2020 deployment. The inversion method is applied with a final solution vertical resolution of 10 m for the Nortek system and 20 m for the RDI system. A coarser vertical resolution was needed for the RDI system to include a larger number of quality data points in each final solution bin. Data from the RDI system

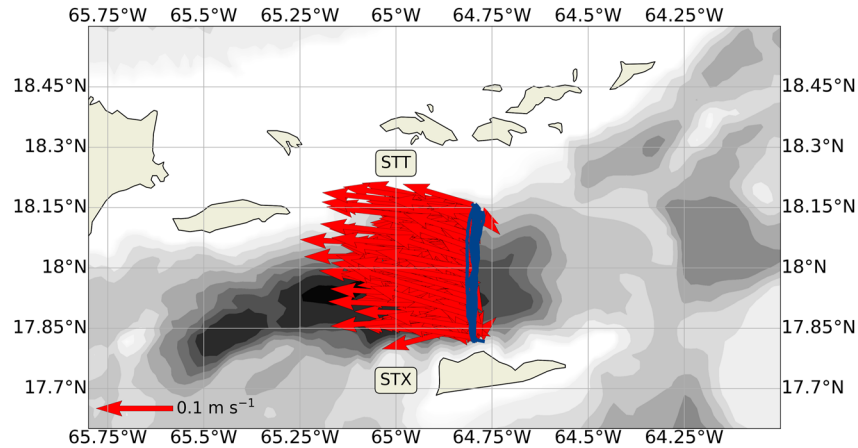

Figure 3. Glider transect track (blue) and segment depth-average current vectors (red) from the October-2020 St. Thomas-St. Croix, Anegada Passage deployment.

experienced degraded data quality with depth likely due to less energy being emitted into the water column and thus a poorer return, especially with decreased scatterers with depth.

The DAC estimate is an integral constraint on the inversion method derivation of absolute horizontal water velocity. DACs can be impacted by a variety of factors such as errors in the internal compass and attitude sensors, accuracy of the hydrodynamic flight model, internal waves, and biofouling (Rudnick et al., 2018). Despite these potential sources of error, DAC root-mean-square accuracy is estimated to be approximately 0.01–0.02 m s^{-1} (Rudnick et al., 2018). This uncertainty is minimal compared to the magnitude of the bulk transport estimates reported here. Furthermore, Todd et al. (2017) apply a quality control step for correcting an instrumental heading bias, which are typically observed in individual velocity profiles as an erroneous heading-dependent shear. Following this correction, substantially smaller heading bias' were found for each deployment presented here to the extent that corrections were not necessary.

For the 2020 and 2022 deployments, horizontal water velocity profiles derived for each glider segment are interpolated onto a regular depth, longitude, and latitude grid representing the mean position of the glider transects between St. Thomas and St. Croix. Glider drift in the E/W direction was minimal so a constant longitude of 64.80° W was chosen. The N/S extent of the transect lines is approximately 30 km. Glider speed over ground for these deployments was consistently ∼1 km/hr where a single 1000-m segment (dive and climb) transited ∼3 km. Six equally spaced latitude bins (roughly 5 km apart) were chosen so that 2–3 glider segment would be included in the interpolation. This grid interpolation effectively smoothes the absolute velocities. After the velocity profiles are interpolated onto the regular grid, E/W velocity is integrated over the full water column and transect length to produce transport in units of Sverdrups (where 1 Sv = 10^6 m^3/s). Deployment average transport and standard deviation are obtained by calculating transport mean and standard deviation over the total number of transects. E/W transports reported here are effectively cross-passage transport due to the orientation of the transects. There was no attempt to remove tidal variability from the observations. Tides have low spatial variability in this region and are either diurnal or semidiurnal with a relatively small amplitude, typically less than 10-cm (Kjerfve, 1981; Wilson & Johns, 1997). Averaging over the spatial (3-km glider segments, 30-km transects) and temporal (1-hr glider segments, ∼36-hr transects) length scales of these observations is assumed to remove tidal variability.

For the 2021 deployments, horizontal water velocity profiles are derived for each glider segment but are not interpolated onto a regular depth, longitude, and latitude grid as there is only one transect per deployment. Because the deployment tracks were designed to travel in a cross-passage direction, the 2021 absolute velocity data are rotated by the orientation of the passage opening (∼18°). This rotation transforms the E/W velocity into cross-passage velocity, which enables a more direct comparison with the cross-glider track geostrophic velocities detailed in the following section. This rotation is not needed for the 2020 and 2022 deployments because these tracks were in an approximately N/S direction, so the cross-glider track geostrophic velocities are approximately in a cross-passage direction. Transport is derived for the 2021 deployments by using the start and end locations of each segment to calculate distance in meters and then cross-passage velocity is integrated over the full water column and transect length to produce transport in units of Sverdrups.

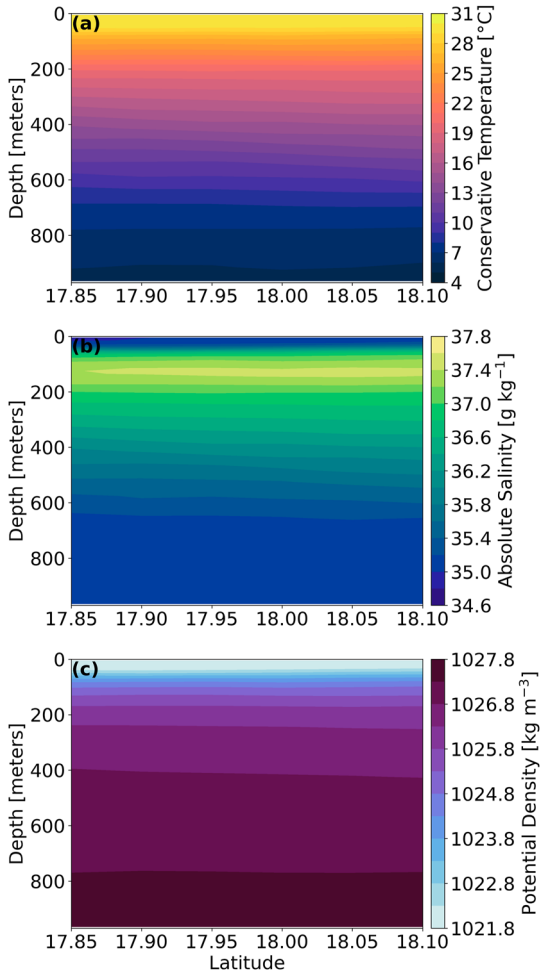

Figure 4. Example conservative temperature (a), absolute salinity (b), and potential density (c) transects in the STT-STX section of the Anegada Passage interpolated onto the regular depth-latitude-longitude grid for thermal wind geostrophic velocity calculation.

2.2. Transport From Geostrophic Velocity

Geostrophic velocity is estimated via the thermal wind relationship following the methodology by Høydalsvik et al. (2013). The CTDs on both gliders were sampled every 2 s throughout full dives and climbs. Potential density (σ_θ, from here on: density) is calculated from conservative temperature (Θ, from here on: temperature) and absolute salinity (S_A, from here on: salinity) measurements using the TEOS-10 standard (Roquet et al., 2015). For the 2020 and 2022 deployments, measurements from dives and climbs were averaged in 2-m vertical bins and interpolated onto the same depth, longitude, and latitude grid used for calculating transport from the current profiler data both to reduce noise and facilitate comparisons. For the 2021 deployments, measurements from dives and climbs were also averaged in 2-m vertical bins but no interpolation onto a regular grid was needed because these deployments were on their own unique tracks. Figure 4 shows an example of temperature, salinity, and density on this grid for the 2020 deployment. Density measurements are then used in the thermal wind relationship to calculate the cross-glider track component of the geostrophic vertical shear:

$$\frac{\partial u}{\partial z} = \frac{g}{\rho_o f}\frac{\partial \rho}{\partial y} \tag{2}$$

where u is the cross-glider track velocity, z is the vertical coordinate, g is the acceleration due to gravity, ρ_o is a reference density (1,027 kg/m^3), f is the Coriolis parameter, ρ is density, and y is the along-track distance. Along-track distance is taken to be the distance between the latitude bin edges for the 2020 and 2022 deployments, roughly 5 km, and true along-track distance for the two 2021 deployments. Relative cross-glider track geostrophic velocity (U_{relative}) is obtained by integrating the previous equation with respect to z:

$$U_{\text{relative}} = \int_{-H}^{0} \frac{g}{\rho_o f}\frac{\Delta \rho}{\Delta y} \tag{3}$$

where H is the maximum dive depth of the glider. Glider dead-reckoned, depth-average currents (U_{DAC}) used to constrain the ADP velocity profiles are also interpolated onto the latitude grid used here. Interpolating the depth-average currents onto this grid effectively results in one representative DAC to be used as a constraint for each latitude point a given transect. For the 2021 deployments, the true DAC is used as a constraint for each glider segment. The depth-average currents are used to reference the relative cross-glider track velocity to absolute geostrophic velocity ($U_{\text{geostrophic}}$) by:

$$U_{\text{geostrophic}}(y,z) = U_{\text{relative}}(y,z) + U_{\text{reference}}(y) \tag{4}$$

The reference velocity is calculated from the DAC as:

$$U_{\text{reference}}(y) = U_{\text{DAC}} - \frac{1}{H}\int_{-H}^{0} U_{\text{relative}}(y,z)dz \tag{5}$$

In smaller passages in the southern Caribbean where the flow is expected to have a stronger ageostrophic component, Wilson and Johns (1997) found that smoothing of geostrophic velocity estimates greatly improved comparisons with measured velocities. It was necessary to interpolate the density fields onto the regular grid for the 2020 and 2022 deployments due to the repeating transects, which effectively smoothed these geostrophic velocity estimates. The geostrophic velocity estimates from the 2021 deployments were smoothed using a local least-squares fit by a third degree polynomial in an approximately 30 km rolling filter window similar to Todd et al. (2011). After geostrophic velocity profiles are calculated they are integrated over the full water column and transect length to produce transport in units of Sverdrups. Deployment average transport and standard deviation are calculated in the same manner as was done for the ADP directly measured velocities.

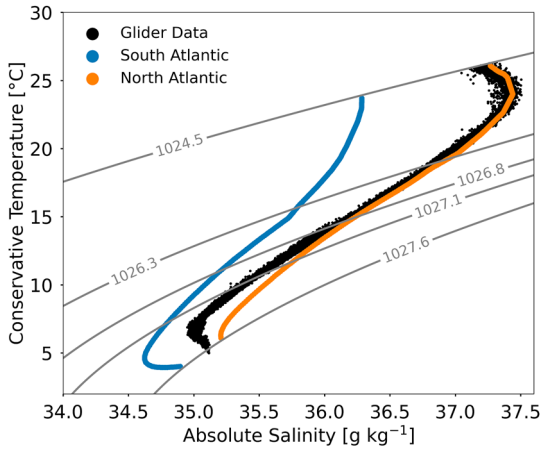

Figure 5. Representative source water mass profiles obtained using mean temperature and salinity profiles from World Ocean Atlas 2018 following Rhein et al. (2005) for the South Atlantic (blue) and North Atlantic (orange). Temperature and salinity data from all four glider deployments shown in black.

2.3. Water Mass Analysis

Water mass analyses using temperature and salinity have been used widely throughout the Atlantic in the past (Poole & Tomczak, 1999; Schmitz & McCartney, 1993; Schmitz & Richardson, 1991) and can applied in a manner to distinguish SAW from NAW in the Caribbean inflow (Garraffo et al., 2003; Johns et al., 2003; Kirchner et al., 2008; Mertens et al., 2009; Rhein et al., 2005). Here, a water mass analysis is conducted following Rhein et al. (2005) by taking an isopycnal mixing approach and expanded through the use of least-squares fitting. Temperature and salinity data are used as constraints in the following system of equations to solve for the mixing fraction of NAW or SAW that is necessary for the observed data to be derived from two distinct source waters.

$$x_{SA}T_{SA} + x_{NA}T_{NA} - T_{obs} = R_T \quad (6)$$

$$x_{SA}S_{SA} + x_{NA}S_{NA} - S_{obs} = R_S \quad (7)$$

$$x_{SA} + x_{NA} - 1 = R_{MC} \quad (8)$$

Here, (T_{SA}, S_{SA}, T_{NA}, S_{NA}) represent the temperature and salinity definitions for the distinct source water types from the South Atlantic and North Atlantic; (T_{obs}, S_{obs}) represent the observations; (x_{SA}, x_{NA}) represent the fractional relative contributions; and (R_T, R_S, R_{MC}) represent the residuals which are minimized through a least squares fitting. This method is similar to the optimum multiparameter (OMP) analysis but is limited in the number of source water masses (two) than can be used to still have a determined system of equations. Poole and Tomczak (1999) used OMP analysis to distinguish six source water mass endpoints from three linear T/S relationships in the Atlantic Central Waters (one northern type and two southern types) and constrained this resulting system of equations by including oxygen, silicate, nitrate, and phosphate data along with temperature and salinity. Here, we follow Rhein et al. (2005) and refrain from separating the two South Atlantic source water types which allows for the calculation of fractions of SAW and NAW by T/S data alone. The Python package PYOMPA (version 0.3) is adapted for this analysis (Shrikumar et al., 2021).

The isopycnal mixing analysis is applied from $\sigma_\theta = 24.5$ (~110 m) to $\sigma_\theta = 27.5$ (~1,000 m) which is the glider's maximum operational depth. Representative source water mass profiles are obtained using mean temperature and salinity profiles from World Ocean Atlas 2018 (WOA18; Locarini et al., 2018; Zweng et al., 2018) following the locations of the hydrographic data used by Rhein et al. (2005). The in-situ temperature and salinity profiles from WOA18 are converted to conservative temperature and absolute salinity using the TEOS-10 standard that was applied to the glider data (Roquet et al., 2015). Figure 5 shows these profiles along with all glider temperature and salinity observations below the surface layer analyzed here. The isopycnal water mass analysis is conducted at each depth interval (steps of 2-m vertically) from the respective glider deployments discussed above. At these depth intervals, the T/S properties from the two source water masses along the same isopycnal are used to compute the fraction of each endmember needed to obtain the properties of the observed data. We follow the water mass density ranges and naming conventions of Stramma and Schott (1999) and Rhein et al. (2005) where SW is $\sigma_\theta < 24.5$, salinity maximum water (SMW) is $24.5 \geq \sigma_\theta < 26.3$, upper central water (uCW) is $26.3 \geq \sigma_\theta < 26.8$, lower central water (lCW) is $26.8 \geq \sigma_\theta < 27.1$, and intermediate water is (IW) $27.1 \geq \sigma_\theta < 27.6$. Details regarding differences between the respective North Atlantic and South Atlantic component of each water mass are outlined further in the discussion. The fractional contributions of each source water mass (x_{SA}, x_{NA}) are multiplied by the absolute velocity derived transport at each depth interval to obtain SAW and NAW transport.

The implications of the choices for these source water types have been detailed extensively (Kirchner et al., 2008, 2009; Mertens et al., 2009; Rhein et al., 2005), however we emphasize again that the South Atlantic SMW source water used here is a fresher endmember from the eastern South Atlantic. The more saline SMW from the western South Atlantic is nearly indistinguishable from the North Atlantic SMW. We acknowledge that this choice neglects the contribution of high salinity SAW to the total SAW transport in the SMW layer and estimate potential contributions from this water mass using mass balance assumptions in the discussion (Kirchner et al., 2008; Rhein et al., 2005; Zhang et al., 2003).

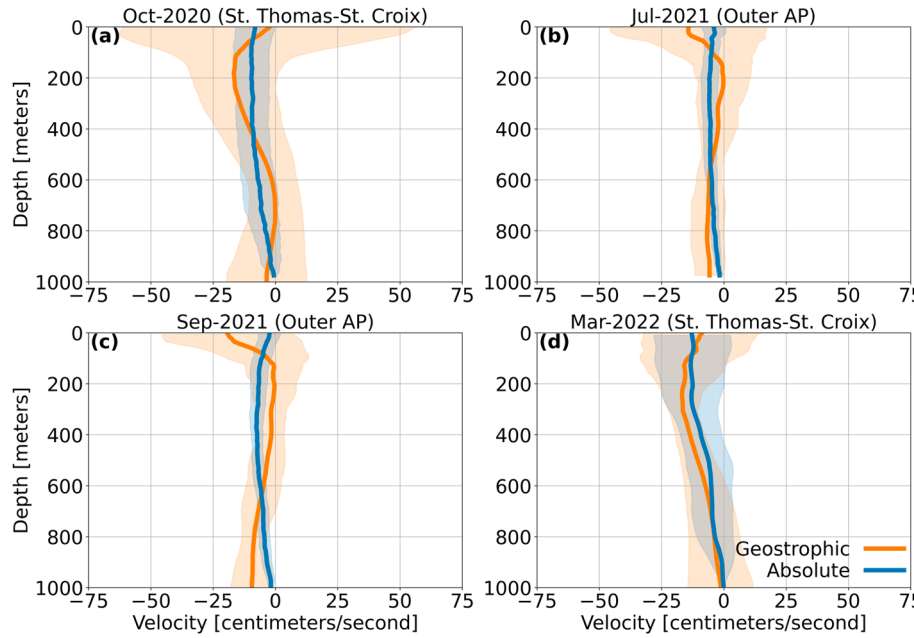

Figure 6. Mean thermal wind derived geostrophic velocity (orange) and acoustic doppler profilers derived absolute velocity (blue) shaded by one standard deviation for all four deployments. Profiles for the 2020 and 2022 deployments represents E(+)/W(−) velocity and cross passage (- into/+ out of passage) velocity for the 2021 deployments.

The isopycnal water mass analysis cannot be applied to the surface layer. Therefore, we follow the assumptions made by SR91, Schott et al. (1998), Hellweger and Gordon (2002), and Rhein et al. (2005) and the subsequent studies that have since adopted the methodology used by Rhein et al. (2005) for this layer. These studies have found that the tropical surface waters warmer than 24°C ranging from the equatorial Atlantic to the Florida Straits are of South Atlantic origin. Thus, here we assign all transport in the $\sigma_\theta < 24.5$ layer as SAW.

3. Results

3.1. Current Structure and Transport

Figure 6 shows mean velocity profiles with a one standard deviation shading for both geostrophic velocity and ADP derived absolute velocity for all four deployments. These mean velocity profiles show the flow is largely barotropic. There is an overall agreement on the mean velocity direction into the Caribbean with larger variability in the geostrophic velocity estimates. Differences between geostrophic and absolute velocity estimates will be discussed further in the following section.

The two 2021 deployments occupied somewhat different transect lengths and orientations, but both generally sampled the entire AP (Figure 2). The first 2021 AP transect, located in the furthest northeast corner of the study area, was occupied from July 4-9, 2021. The ADP derived absolute velocities observed during this glider deployment were also predominately into the Caribbean (Figure 7a). The flow had a slight along passage component, roughly aligned with the shelves on both edges of the transect (Figure 7c). The flow was mainly barotropic, with a slight shearing of the along passage component of the flow occurring near the bathymetric feature Dog Knoll. The average transport was −4.43 Sv into the Caribbean.

The second AP transect, traveling from the area of the St. Thomas-St. Croix transects to approximately 50 km south of Dog Knoll, was occupied from September 14-18, 2021. The ADP derived absolute velocities observed during this glider deployment were predominately into the Caribbean, with a weak reversal in the middle of the transect (Figure 7b). There was more variability in the along passage component of the flow during this deployment, though the magnitude was substantially less than the first deployment (Figure 7d). Again, the flow was mainly barotropic, with a slight shearing of the along passage component of the flow over the entire transect. The average transport was −5.24 Sv into the Caribbean. The mean cross passage velocity for both transects was

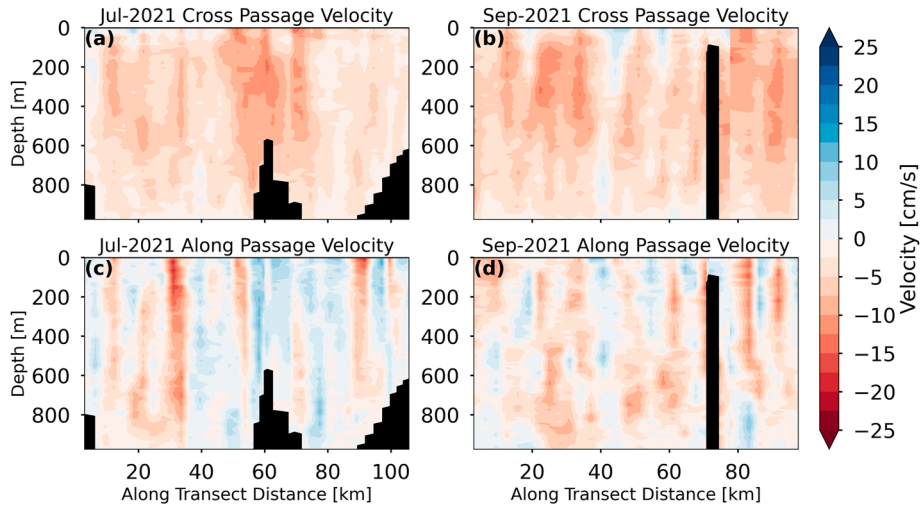

Figure 7. Anegada Passage velocity derived from glider mounted acoustic doppler profilers for the first 2021 deployment (left column) and second 2021 deployment (right column) in the cross passage (- into passage/into Caribbean, + out of passage/into Atlantic) direction (top row) and along passage (- toward bottom of passage/south, + toward top of passage/north) direction (bottom row). Both transects started on the E/NE side of the passage and traveled to the W/SW side of the passage. The duration of the July-2021 deployment was approximately 5.5 days and the duration of the September-2021 deployment was approximately 4.5 days.

approximately −5 cm s^{-1} with a maximum around −20 cm s^{-1} and little to no reversal of the flow. The mean along passage velocity for both transects was approximately zero with a maximum around ±15 cm s^{-1}. If values for both transects are averaged, the averaged transport observed here is −4.84 Sv into the Caribbean.

Transport time-series' were calculated from the ADP derived absolute velocities collected on the repeat transect lines between St. Thomas and St. Croix during the 2020 and 2022 glider deployments (Figure 8). Mean transport values for the 2020 and 2022 deployments are within each other's error bars, despite more than double the number of transects being occupied in 2020 compared to 2022 (15 vs. 6). Within a deployment and comparing the two deployments, there is very little variability about the mean transport value, suggesting these means are relatively robust. As with the 2021 deployments, the flow here is predominately westward into the Caribbean, with little to no northward component. If values for the 2020 and 2022 deployments are averaged together, the mean transport observed here is −2.33 ± 0.71 Sv into the Caribbean.

Transport values were also derived for each transect from cross-glider track geostrophic water velocities and then averaged for each deployment (Table 1). The mean geostrophic transport for the 2020 deployment is within the error bars of the 2020 deployment absolute velocity transport value. While no standard deviation estimates are available for the 2021 deployments, there is a general agreement on transport into the Caribbean. Furthermore,

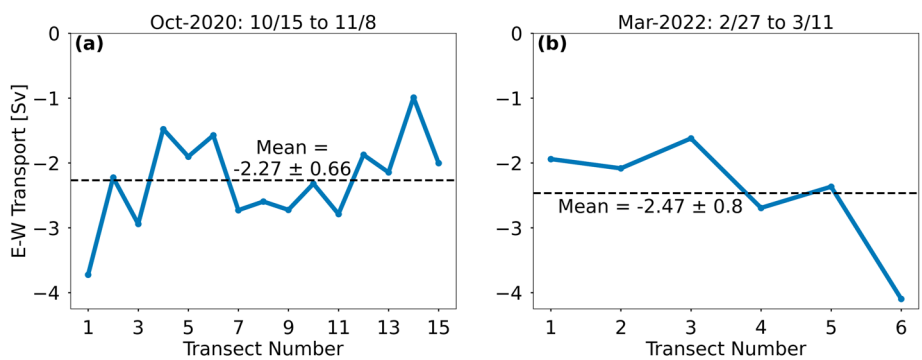

Figure 8. Acoustic doppler profilers derived absolute E(+)/W(−) transport time-series' calculated from the repeat transect lines between St. Thomas and St. Croix for the RU29 October 2020 deployment (a) and RU36 March 2022 deployment (b). Black dashed line represents the deployment mean transport. A single transect consistently took approximately 36 hr.

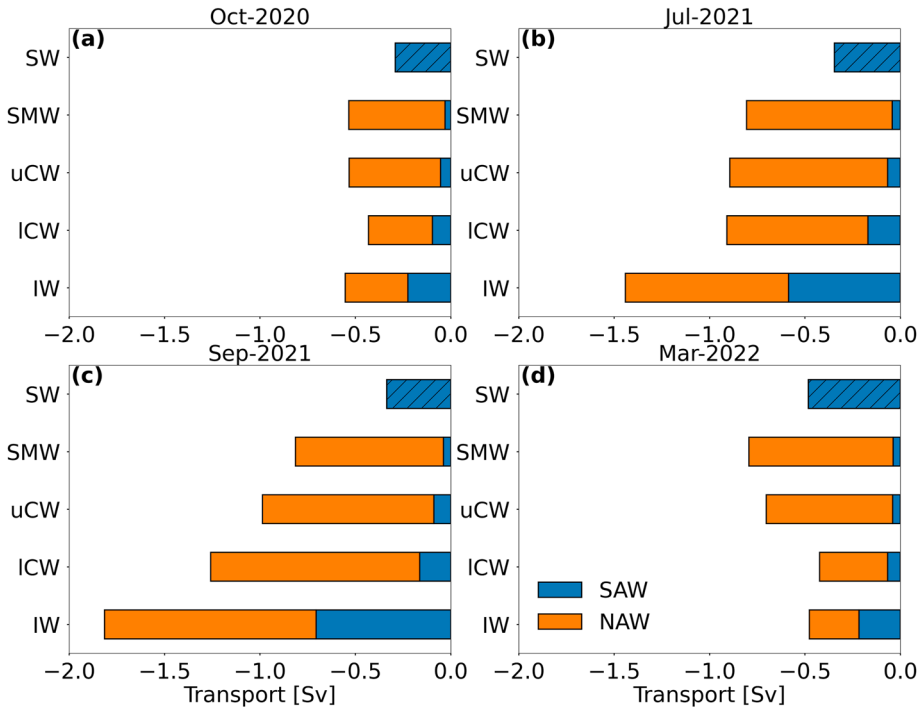

Figure 9. Transport of South Atlantic Water (blue) and North Atlantic Water (orange) in the major water masses from the isopycnal water mass analysis for the four glider deployments. The surface water is hatched blue as it was not included in the water mass analysis. The October-2020 and March-2022 data represent means of the repeat STT-STX transects.

the mean geostrophic transport for the 2022 deployment is outside the error bars of the 2022 absolute velocity transport value, though there is general agreement on transport into the Caribbean here as well.

3.2. Water Mass Analysis and Transport

Following the isopycnal water mass analysis, NAW and SAW transport is calculated per water mass for each deployment (Figure 9). The uncertainties provided below are due to the formulation of a single representative property value (e.g., SAW transport, percentage of SAW in each water mass layer, etc.) for the AP from all four deployments. Including the surface layer, the total SAW transport for each deployment is October-2020: −0.70 Sv, July-2021: −1.21 Sv, September-2021: −1.33 Sv, and March-2022: −0.84 Sv (mean = −1.02 ± 0.26 Sv), which represents 25%–34% of the respective deployment transports (Table 1, mean = 29 ± 3%). The surface layer accounts for the transport of −0.29 to −0.48 Sv of SAW, which represent 8%–20% of the total transport (mean = 11 ± 5%) and 25%–57% of the total SAW transport (mean = 38 ± 13%) for the respective deployment transports.

Excluding the surface layer, the relative percentage of SAW versus NAW gradually increases moving from SMW down to IW. For clarity, only the percentage of SAW is reported here as the percentage of NAW simply reflects the remaining percentage. The SMW is overwhelmingly dominated by NAW, with SAW representing 5 ± 0.4% of the total transport in this layer across all four deployments. The uCW layer is also dominated by NAW. SAW represents 8 ± 1.6% of the total transport in this layer across all four deployments. The percentage of SAW in each respective water mass continues to increase into the lCW layer and below. In the lCW layer, SAW represents 17 ± 3.4% of the total transport in this layer across all four deployments. The IW layer has a much more even split between SAW and NAW. SAW represents 41 ± 2.4% of the total transport in this layer across all four deployments. The relative percentage of SAW or NAW in each water mass is largely consistent across deployments indicated by the low standard deviations. Differences in SAW or NAW transport in these water masses across the deployments can be attributed to the differences in the bulk water mass transport from deployment to deployment.

Characteristic temperature and salinity profiles for this region show dominant features such as freshwater barrier layers and high upper ocean heat content and the approximate ranges of the major water masses (Figure 10). The

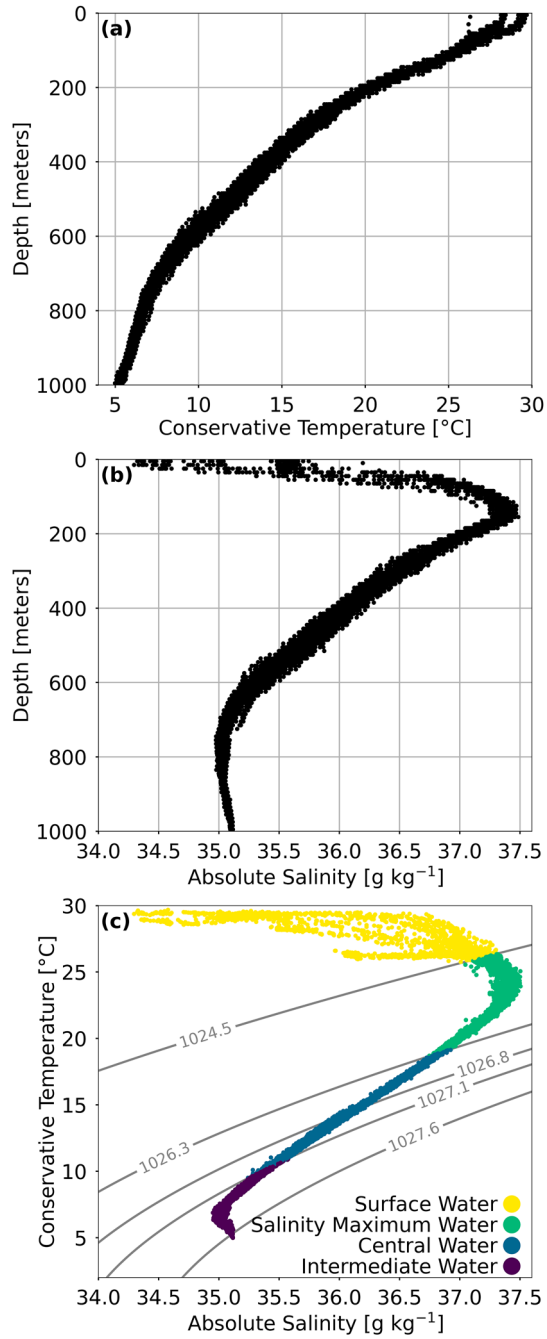

Figure 10. Temperature (a) and salinity (b) profiles in the Anegada Passage region, as well as approximate ranges of the major water masses (c) from all four glider deployments combined.

transport of specific water masses with unique source water types that distinguish their hemisphere of origin within the ranges highlighted in Figure 10 likely play an important role in determining the subsurface density structure of the upper limb of the AMOC. The implications of this balance, the transport of SAW and NAW in these different water masses, are discussed in the following section.

4. Discussion

4.1. Current Structure and Transport

In this study we present glider-based observations of subsurface velocity and integrated transport in the AP that have remarkable similarities with ship-based observations from previous literature. This comparison provides compelling evidence for glider mounted ADPs as a viable alternative to ship-based measurements from ship-mounted ADPs (Johns et al., 1999; Kirchner et al., 2008), lowered-ADPs (Johns et al., 2002), and geostrophic estimates (Metcalf, 1976; Morrison & Nowlin, 1982). While the two 2021 deployments in the AP were single passage crossings, they were intended to be more exploratory in nature, following intentionally similar transects to the two transects in Johns et al. (1999) and consequently provide a particularly valuable comparison point. The magnitude of the subsurface velocity observations from the 2021 deployments agrees well with the magnitude of the observations from the second transect presented in Johns et al. (1999). The 2021 deployments also showed similar structure as subsurface velocity maxima and weak counterflows were common. The magnitude of the subsurface velocity observations from the 2021 deployments were noticeably smaller than the first transect presented in Johns et al. (1999). This difference is likely due to the extremely high velocities in excess of 1.1 m s^{-1} that were highlighted as potentially skewing the observations in Johns et al. (1999).

The observations presented in this study bring to light both potentially new dynamics as well as upper and lower bounds in terms of transport magnitude. Table 1 from Johns et al. (2002) summarized the available transport values and a mean of -2.5 ± 1.4 Sv into the Caribbean was determined for the AP. This value is similar to the -1.8 ± 1.5 Sv mean later reported by Kirchner et al. (2008) but noticeably less than the maximum -8.4 Sv transport observed by Johns et al. (1999) during October 1986. This range in transport estimates and the potential role this flow plays in the pathways and balance of meridional overturning circulation warrant this revisitation of the AP with sustained observations using improved technology. Mean transport values from the St. Thomas-St. Croix transects (-2.27 ± 0.66 Sv and -2.47 ± 0.8 Sv) agree well with the -2.5 ± 1.4 Sv estimate from Johns et al. (2002). However, considering these estimates are more representative of what is historically referred to as the Anegada-Jungfern Passage, or a subset of the greater AP, it is reasonable to expect these values actually represent an underestimation of the total AP transport.

Though these transport estimates may be an underestimate, the repeating St. Thomas-St. Croix transects provide a time-series that sheds light on the variability of this inflow. The means and standard deviations of E/W transport are similar between the October and March deployments. A single transect takes approximately 1.5 days, which suggests the AP transport is stable on weekly time scales. In both the 2020 and 2022 deployments, there is one transect that has a transport value approximately -4 Sv. Though these transport values are greater than one standard deviation from their respective deployment mean transports, they are due to a larger barotropic E/W transport as the N/S component of the glider estimated DAC from these transects are essentially zero. It is also noteworthy that the standard deviation for the

glider-based transport estimates (0.66 and 0.8 Sv) are approximately half of the ship-based estimates (1.4 Sv). Part of the reason the standard deviations are likely smaller is because there are 2–3 times more glider-based transport values used for these calculations when compared with the ship-based estimates. The large number of glider observations further highlights gliders with ADPs as a viable, if not potentially more accurate, method for measuring island passage transport.

To place the glider-based transport estimates presented in this study into the context of prior transport estimates in the region, it is important to understand how these observations were collected. First, it is noteworthy that the transport estimates from Johns et al. (1999) were derived from ship mounted ADPs with a range of only 200 m Kirchner et al. (2008) occupied the AP using a ship-mounted ADP with a range of 1400 m. However, this occupation was only for one transect and resulted in a near-zero transport estimate. The -1.8 ± 1.5 Sv mean transport values for the AP was derived by Kirchner et al. (2008) from combining this single, near-zero transport measurement with the five occupations detailed by Johns et al. (2002). Full-depth, lowered-ADPs were only used by Johns et al. (2002), however they only reported transport estimates per deployment and provided no additional details of the flow. The subsurface velocity data presented in this study then represent the first detailed, published observations of AP inflow below the 200-m profiles reported by Johns et al. (1999). This result is noteworthy because transport below 200 m accounts for anywhere from 20% to 50% of this study's 1,000-m transport estimates.

Previous literature has shown there is a common baroclinic velocity structure in Caribbean passage transports, where the upper 200 m contains approximately half of the respective full passage transport (Johns et al., 1999; Wilson & Johns, 1997). With this observation, Johns et al. (1999) applied a factor of 2 to their upper 200-m transport to estimate total passage transport. To better compare our 1000-m transport estimates, we can therefore multiply the 200-m, −2.4 Sv transport value reported by Johns et al. (1999) by a factor of two. This exercise leads to a −4.8 Sv transport estimate that is in much better agreement with the −4.43 and −5.24 Sv transport estimates (mean = −4.84 Sv) for the two 2021 outer AP deployments reported here. A total AP transport of −4.84 Sv for the outer AP also implies that roughly one-half of the transport is split to the north and south of St. Croix as the mean transport north of St. Croix is −2.33 Sv. Therefore, while the two 2021 transport values are only from one occupation, potentially more influenced by tidal and/or spatial impacts, there is reason to believe the actual bulk, mean AP transport is closer to −4.8 Sv. If the St. Thomas-St. Croix deployment transports are taken to be roughly ½ of the total transport and thus multiplied by a factor of 2 (October-2020 = −4.54 Sv, March-2022 = −4.94 Sv), the mean AP transport across all four deployments can be approximated to be -4.8 ± 0.32 Sv. This implies that the AP transport is larger than previously estimated (−2.5 Sv) and, if confirmed through additional transects across the greater AP, would represent close to 20% of the total Caribbean inflow (−28 Sv). The implications of a potentially larger transport and the transport depth structure in relation to different water masses is discussed in further details in the subsequent section.

There is a general agreement in velocity profiles and transport magnitude between the cross-glider track geostrophic velocities and the ADP derived absolute velocities for all four deployments. This is likely due to the flow being largely barotropic and the glider's DAC being used as a constraint for both the geostrophic and absolute velocity estimates. Ageostrophic effects expected in Caribbean passages (friction, curvature, confluence, internal waves, etc.) are less important in the AP as it is the largest passage. Regardless, averaging the repeat transects serves to smooth some of this variability, which is desired when discussing a bulk representation of the flow as we present here. In smaller passages, where these ageostrophic effects have caused disagreement between geostrophic and absolute velocities, averaging repeat transects and smoothing both the absolute velocities and density fields used to calculate geostrophic velocities has led to improvements (Wilson & Johns, 1997).

4.2. Contributions From the Surface Waters to the SAW Transport

In the results presented here for the surface layer, we follow the assumption that the tropical SW is entirely of South Atlantic origin (Hellweger & Gordon, 2002; Kirchner et al., 2008, 2009; Mertens et al., 2009; Rhein et al., 2005; Schmitz & Richardson, 1991; Schott et al., 1998). In their analysis of the sources of the Florida Current, SR91 were the first to consider tropical surface waters warmer than 24°C and waters in the 7–12°C range to be of South Atlantic origin. They used these temperature ranges in their analysis to estimate that ∼45% of the Florida Current transport may originate in the South Atlantic. While a more detailed and accurate water mass analysis using temperature and salinity data is now conducted for the water masses below the surface layer, we adopted the assumption made by SR91 for the surface layer as the isopycnal water mass analysis

cannot be applied here. The following interpretation of the results depends only partially on this assumption as the surface layer here accounts for the transport of −0.29 to −0.48 Sv of SAW (mean = −0.36 ± 0.07 Sv), which represents a mean of only 12 ± 5% of the total transport and 38 ± 13% of the total SAW transport reported here. The surface layer contributing 38% of the transport of SAW in the AP is less than the over 50% contribution from the surface layer to the total SAW transport in the passages south of Guadeloupe from Rhein et al. (2005).

4.3. Contributions From the Saline South Atlantic SMW to the SAW Transport

In the SMW layer, the low salinity endmember from the eastern South Atlantic contributes 5 ± 0.4% which is noticeably smaller than the 30%–37% found by Rhein et al. (2005) in the passages south of Guadeloupe. As the isopycnal water mass analysis only permits two source water masses, the saline SMW from the western South Atlantic cannot be distinguished from the North Atlantic SMW and is consequently unaccounted for. Several methods have been applied to estimate contributions from the western South Atlantic SMW source. Zhang et al. (2003) used potential vorticity, salinity, and geostrophic flow maps to determine the transport pathways for waters with densities between $\sigma_\theta = 23.2$ and $\sigma_\theta = 26.0$ between the Subtropical and Tropical Atlantic in both hemispheres. Transports of 2–3 Sv and 4–6 Sv were determined for the saline North Atlantic and saline South Atlantic SMW, respectively. Using this mass balance and converting it to a fraction, Rhein et al. (2005) proposed that the saline western South Atlantic SMW could contribute 47%–54% of the North Atlantic SMW transport. Kirchner et al. (2008) expanded on the approximation made by Rhein et al. (2005) by conducting an isopycnal water mass analysis off the Brazilian coast to 40°W and between 5°S and 7°N. They determined that the fraction of the transport of the low salinity eastern South Atlantic endmember is on the order of 70%–75%, leaving a maximum of 25%–30% from the saline western South Atlantic. Using these estimations, a factor of 25%–54% could reasonably be applied to the NAW component of the SMW transport to account for the saline western South Atlantic source. With these ranges from prior literature, the potential total SAW fraction from both sources, with the 5% observed in this analysis for the fresh endmember, would then sum to 30%–59%. However, using both hydrographic and model data, Kirchner et al. (2009) determined that the low salinity endmember from the eastern South Atlantic dominates the equatorial region and prevents the saline western South Atlantic SMW from spreading northward. Therefore, it is expected that contributions from the saline western South Atlantic SMW in the AP are toward the lower end of this estimate range. Taking the minimum from this range (25%), applying it to the North Atlantic component of the SMW for the respective deployments, and including this additional SAW contribution would increase the total SAW transport for each deployment to October-2020: −0.83 Sv, July-2021: −1.40 Sv, September-2021: −1.52 Sv, and March-2022: −1.03 Sv (mean = −1.20 ± 0.28 Sv).

4.4. Total Transport of SAW Into the Caribbean

If a conceptual box model is applied to the greater Caribbean Sea, there are constraints on the through-flow that reveal unresolved aspects of the AMOC return flow here. Figure 1 may be helpful to geographically guide the reader through this section. The presence of SAW in the northern hemisphere represents AMOC return flow. Through the use of the isopycnal water mass analysis used in this analysis, Rhein et al. (2005) estimated that a maximum of 11 Sv of SAW is flowing into the Windward Island Passages of the southern Caribbean. At 26°N, it is accepted that the strength of the AMOC is 17 Sv (Frajka-Williams et al., 2019). This implies that there are 17 Sv of SAW flowing northward through the Florida Straits at 26°N. With these values as the input and output for this conceptual box model, the pathways for the remaining 6 Sv of SAW entering the Caribbean north of the Windward Island Passages and exiting through the Florida Straits are highlighted as largely unresolved.

If the mean value of −1.20 ± 0.28 Sv from the proposed addition of the saline western South Atlantic SMW is taken as the estimate for the total SAW transport through the AP, this would represent 20% of the 6 Sv of SAW entering the Caribbean north of the Windward Island Passages. However, if the St. Thomas-St. Croix transects are again considered to be representative of ½ of the total AP transport as proposed in Section 4.1, the SAW transports for those deployments would increase the October-2020 deployment to −1.66 Sv and the March-2022 deployment to −2.06 Sv. These values are in much better agreement with the −1.40 Sv for the July-2021 and −1.52 Sv for September-2021. This would bring the mean total SAW transport through the AP up to −1.66 ± 0.25 Sv which would represent 35% of the mean total AP transport reported here (−4.8 Sv) and 28% of the −6 Sv of SAW entering the Caribbean north of the Windward Island Passages.

We show here that the AP is of a larger importance for the inflow of SAW into the Caribbean than previously considered. While transport in the 5–12°C range has historically been attributed largely to the AP due to its deep sill depth (Schmitz, 1995; Schmitz & McCartney, 1993; Wilson & Johns, 1997), Kirchner et al. (2008) is the only reference to consider SAW transport throughout the entire AP through a detailed water mass analysis with co-located transport measurements. This analysis found 0 Sv of SAW transport in observational data and −0.4 Sv of SAW transport in modeled data, both of which are significantly less than the SAW transport values reported here. This difference is likely due to two factors. First, these authors reported a total AP transport of -1.8 ± 1.5 Sv that is lower than the previously accepted value of -2.5 ± 1.5 Sv (Johns et al., 2002) and considerably lower than -4.8 ± 0.32 Sv proposed in this analysis. Second, Kirchner et al. (2008) reported the fraction of SAW in the IW layer to be 21% in their observational data and 38% in their modeled data, both of which are lower than the mean of 41% proposed in this analysis.

4.5. Transport of NAW Into the Caribbean

NAW that recirculates in the North Atlantic subtropical gyre and does not represent any part of the cross-equatorial AMOC return flow still makes up a substantial portion of the transport of the Florida Current and thus must be entering the Caribbean through either the Greater Antilles, Leeward Island, or Windward Island Passages. Following SM17, the water mass with the highest respective transport in the Florida Current is found in what they refer to as intermediate water east (IWE; 14.8 ± 0.2 Sv) water mass class. IWE is comprised of NAW SMW, eighteen-degree water (EDW; Worthington, 1958), and North Atlantic Central Water, all of which have origins in the North Atlantic. This water mass class is considered to be mid-depth waters $24 \geq \sigma_\theta < 27$, above the IW layer and encompassing the SMW, uCW, and lCW layers discussed here. If NAW transport in the SMW, uCW, and lCW layers is summed for each deployment, here considering the entirety of North Atlantic SMW as to formulate an upper limit, the IWE transport in the AP could account for −1.32 Sv for October-2020, −2.33 Sv for July-2021, −2.77 Sv for September-2021, and −1.77 Sv for March-2022 (mean = -2.05 ± 0.55 Sv). A mean of −2.05 Sv would represent 14% of the IWE in the Florida Current. If the St. Thomas-St. Croix transects are again considered to be representative of ½ of the total AP transport as proposed in Section 4.1, the IWE transports for those deployments would increase the October-2020 deployment to −2.64 Sv and the March-2022 deployment to −3.54 Sv. These values are in much better agreement with the −2.33 Sv for the July-2021 and −2.77 Sv for September-2021. This would bring the mean total IWE transport through the AP up to -2.82 ± 0.45 Sv which would represent almost 19% of the IWE in the Florida Current.

4.6. Implications for Water Mass Transport Into the Caribbean

Given the uncertainties and consequences for projected changes in the AMOC (Caesar et al., 2018; Frajka-Williams et al., 2019; Praetorius, 2018; Rahmstorf, 2002; Thornalley et al., 2018) and the fact that the time-series length of our observing systems is just entering the "detection window" for determining statistically significant trends (Lobelle et al., 2020), it is vital to work toward a better understanding of the dynamics of this system. SM17 recently determined that the source of the AMOC flow through the Florida Straits is controlled potentially twice as much by NAW than by SAW. This is further significant as these authors determined decadal changes in salt transport through the Florida Straits may be impacted more by actual salinity changes rather than changes in the transport itself. That is, the Florida Current water mass structure determines the northward transport of salt more than the transport of the Florida Current itself. For example, SM17 found that both NAW and Antarctic Intermediate Water (SAW) have salinified in recent decades which increased the salinity anomaly transport without corresponding changes in the volume transport. Therefore, the transport of SAW and NAW through the Caribbean Island Passages and into the Florida Straits has substantial implications for AMOC heat and salt transport and analyses focused on determining potential upstream changes in the transport of these water masses are needed.

If the −1.66 Sv of SAW transport through the AP are considered with the 11 Sv of SAW transport thought to be flowing in through the Windward Island Passages (Rhein et al., 2005), 12.66 Sv out of the 17 Sv (74%) of cross-equatorial AMOC return flow through the Caribbean are now accounted for. While this leaves the pathways for the approximately 4.34 Sv or 26% of the remaining SAW transport unaccounted for, model analysis from Kirchner et al. (2009) suggests it may enter the Caribbean through either Mona Passage or Windward Passage (between Cuba and Hispaniola, Figure 1). This is further supported by the inconsistencies and potential

corrections SM17 raise on the assumptions SR91 make on SAW transport. If we follow SM17 by not including SW transport as part of the AMOC, the 11 Sv of SAW transported through the Windward Island Passages determined by Rhein et al. (2005) would be closer to 5.5 Sv. The 50% of SAW in the SW layer relative to the total transport through the Windward Island Passages is larger than the 38% found here in the AP. If SW transport is excluded from both the 11 Sv Windward Island Passage inflow and 1.66 Sv AP inflow of SAW (5.5 and ∼0.63 Sv respectively) the inflow of only 6.53 Sv or 38% of the 17 Sv SAW entering the Caribbean and exiting the Florida Straits can be accounted for. This highlights that there may be more uncertainty and unknowns in the cross-equatorial AMOC return flow pathways than previously considered.

With these results, we have shown that SAW transport in the IW layer is larger in the AP compared to other known passage transports for this layer. IW transport occurs almost entirely below 600 m and thus the deep sill depths of the AP (1,915 m) (Fratantoni et al., 1997) and Windward Passage (1,560 m) (Metcalf, 1976) highlight these passages as likely important IW transport pathways.

SM17 distinguish IWW (Intermediate Water West) as potentially contributing a large percentage of the unaccounted for AMOC transport, however the origin of IWW is noted as difficult to determine based on temperature and salinity alone. It is important to note IWW water mass class used by SM17 consists of the SMW, uCW, and lCW reported here and is distinctly different than IW discussed in this water mass analysis. SM17's IWW has been discussed as originating in the Gulf of Mexico (Schmitz & McCartney, 1993), Caribbean (Schmidt et al., 2004), or the tropical or South Atlantic (Rhein et al., 2005). Measurements of additional parameters such as dissolved oxygen and at least one nutrient parameter, depending on the number of unique source waters, that covaries with respiration/remineralization as a water mass is transported and ages could potentially shed light on water mass origin uncertainty through the use of optimum multiparameter (OMP) water mass analysis (Poole & Tomczak, 1999; Tomczak & Large, 1989). If SW transport is excluded from the SAW transport, a revisitation of all Caribbean passages to measure these additional parameters along with subsurface velocity could help to better constrain this uncertainty. Regardless, the results presented here suggest that a major finding of this analysis is the likely non-negligible transport of SAW at mid-depths in the AP.

5. Conclusion

This study presents glider-based observations of upper ocean temperature, salinity, and subsurface velocity in the AP region of the northeastern Caribbean Sea. The glider observations analyzed in this study represent a proof-of-concept for using gliders as a means for measuring island passage transport. These observations of co-located temperature, salinity, and subsurface velocity also represent the first measurements of this kind in this region in nearly two decades. Four glider deployments were conducted in the AP region, two conducting repeat transects between St. Thomas and St. Croix and two conducting single transects across the wider AP. A detailed isopycnal water mass analysis was conducted to quantify the transport of water masses with South Atlantic or North Atlantic origin in the passage transport. We interpret the transport observations collected during these deployments as showing two potentially new aspects of AP transport. The total transport (-4.8 ± 0.32 Sv) and the transport of SAW (-1.66 ± 0.25 Sv) in the AP may be larger than previously estimated, potentially by up to a factor of two for total transport. An AP SAW transport of -1.66 Sv would represent 35% of the mean total AP transport reported here and 28% of the 6 Sv of SAW entering the Caribbean north of the Windward Island Passages. These results also show gliders with ADPs are a viable method for measuring island passage transport.

Sustained observations of Essential Ocean Variables (EOVs; Lindstrom et al., 2012) improve our ability to understand, predict, and assess components of the climate system. EOVs like sea surface temperature and salinity, subsurface temperature and salinity, temperature and salinity anomaly transport, sea level anomaly, and deep density gradients have been linked to changes in the strength of the AMOC (Frajka-Williams et al., 2019; Szuts & Meinen, 2017). In the Caribbean, EOVs are also impacted by variations in the transport of water masses with differing sources and in the variations of the source waters themselves. In light of the uncertainties surrounding the AMOC, as well as the recent evidence of climate change induced impacts on the Caribbean Sea, sustained and expanded observations of these metrics are needed in this region. Observations of EOVs specifically relevant to the dynamic features of this region (heat content, heat transport, freshwater content, freshwater transport, freshwater barrier layer thickness, depth, and magnitude of salinity maximum, etc.) are especially needed.

This study has added to the growing body of literature supporting the use of gliders as an effective component of the global ocean observing system. In the three decades since Henry Stommel's 1989 vision of the Slocum Mission, the depth and endurance range of gliders have advanced, and a growing number of complex instruments are now being integrated regularly. The maturity glider platforms have now reached make them uniquely well suited to collect the "evolving maps of subsurface variables" needed for sustained climate monitoring developed in the original vision of Stommel (1989).

Data Availability Statement

Glider data used in this analysis can be found at https://gliders.ioos.us/ under the following dataset ID's: ru29-20200908T1623, ru29-20210630T1343, ru29-20210908T1943, and ru36-20220223T1807. The acoustic current profiler data collected during these deployments can be found at https://doi.org/10.5281/zenodo.7468695 (Gradone et al., 2022a). The code used for this analysis can be found at https://doi.org/10.5281/zenodo.7473774 (Gradone et al., 2022b).

Acknowledgments

We are grateful for support from the G. Unger Vetlesen Foundation for the 2020 and 2021 deployments and the Office of Naval Research (N00014-20-1-2568) for the 2022 deployment. We thank Dave Aragon, Nicole Waite, and Chip Haldeman from the RUCOOL glider team and Antonio Farchette from OCOVI for assistance preparing, piloting, deploying, and recovering the gliders used in this analysis. J.C. Gradone acknowledges support from the Department of Defense National Defense Science and Engineering Graduate Fellowship. W.D. Wilson acknowledges support from VI-EPSCoR NSF award OIA# 1946412. This is contribution #268 from the Center for Marine and Environmental Studies, University of the Virgin Islands. We thank Eli Hunter and Sam Coakley for assistance with development of the processing codes used in this analysis, Eleanor Frajka-Williams, Rebecca Jackson, and Johannes Karstensen for insightful discussion that guided the water mass analysis, and the anonymous reviewers whose comments helped greatly.

References

Antuña-Marrero, J. C., Otterå, O. H., Robock, A., Mesquita, S., & d, M. (2015). Modelled and observed sea surface temperature trends for the Caribbean and Antilles. *International Journal of Climatology*, *36*(4), 1873–1886. https://doi.org/10.1002/joc.4466

Brambilla, E., & Talley, L. D. (2006). Surface drifter exchange between the North Atlantic subtropical and subpolar gyres. *Journal of Geophysical Research*, *111*(C7), C07026. https://doi.org/10.1029/2005jc003146

Caesar, L., Rahmstorf, S., Robinson, A., Feulner, G., & Saba, V. (2018). Observed fingerprint of a weakening Atlantic Ocean overturning circulation. *Nature*, *556*(7700), 191–196. https://doi.org/10.1038/s41586-018-0006-5

dos Santos, R. A. L., Prange, M., Castañeda, I. S., Schefuß, E., Mulitza, S., Schulz, M., et al. (2010). Glacial-interglacial variability in Atlantic meridional overturning circulation and thermocline adjustments in the tropical North Atlantic. *Earth and Planetary Science Letters*, *300*(3–4), 407–414. https://doi.org/10.1016/j.epsl.2010.10.030

Ellis, D., Washburn, L., Ohlmann, C., & Gotschalk, C. (2015). Improved methods to calculate depth-resolved velocities from glider-mounted ADCPs. In *2015 IEEE/OES eleveth current waves and turbulence measurement (CWTM)*. IEEE. https://doi.org/10.1109/cwtm.2015.7098120

Fischel, A., Seidenkrantz, M.-S., Nürnberg, D., Kucera, M., & Kuijpers, A. (2017). Upper water mass variability in the Anegada/Jungfern Passage NE Caribbean, during the last 11,100 cal. yr. *The Holocene*, *27*(9), 1291–1307. https://doi.org/10.1177/0959683616687378

Frajka-Williams, E., Ansorge, I. J., Baehr, J., Bryden, H. L., Chidichimo, M. P., Cunningham, S. A., et al. (2019). Atlantic meridional overturning circulation: Observed transport and variability. *Frontiers in Marine Science*, *6*. https://doi.org/10.3389/fmars.2019.00260

Fratantoni, D. M., Johns, W. E., Townsend, T. L., & Hurlburt, H. E. (2000). Low-latitude circulation and mass transport pathways in a model of the tropical Atlantic Ocean. *Journal of Physical Oceanography*, *30*(8), 1944–1966. https://doi.org/10.1175/1520-0485(2000)030<1944:llcamt>2.0.co;2

Fratantoni, D. M., Zantopp, R. J., Johns, W. E., & Miller, J. L. (1997). Updated bathymetry of the Anegada-Jungfern Passage complex and implications for Atlantic inflow to the abyssal Caribbean Sea. *Journal of Marine Research*, *55*(5), 847–860. https://doi.org/10.1357/0022240973224148

Garraffo, Z. D., Johns, W. E., Chassignet, E. P., & Goni, G. J. (2003). North BrazilCurrent rings and transport of southern waters in a high resolutionnumerical simulation of the North Atlantic. In G. J. Goni & P. Malanotte-Rizzoli (Eds.), *Interhemispheric water exchange in the Atlantic Ocean* (Vol. 68, pp. 375–409). Elsevier Oceanographic Series.

Glenn, E., Comarazamy, D., González, J. E., & Smith, T. (2015). Detection of recent regional sea surface temperature warming in the Caribbean and surrounding region. *Geophysical Research Letters*, *42*(16), 6785–6792. https://doi.org/10.1002/2015gl065002

Gradone, J., Wilson, D., Glenn, S., & Miles, T. (2022a). Acoustic current profiler data from multi-year (2020–2022) autonomous underwater glider surveys in the Anegada Passage [Dataset]. Zenodo. https://doi.org/10.5281/zenodo.7468695

Gradone, J., Wilson, D., Glenn, S., & Miles, T. (2022b). JGradone/Anegada-glider-transport: v1.0.0 (v3.0.0) [Software]. Zenodo. https://doi.org/10.5281/zenodo.7789790

Gradone, J. C., Hunter, E. J., Mullison, J., & Miles, T. N. (2021). Development of onboard processing capabilities for a Slocum glider acoustic Doppler current profiler. In *Oceans 2021: San Diego Porto*. IEEE. https://doi.org/10.23919/oceans44145.2021.9705895

Gregory, J. M., Dixon, K. W., Stouffer, R. J., Weaver, A. J., Driesschaert, E., Eby, M., et al. (2005). A model intercomparison of changes in the Atlantic thermohaline circulation in response to increasing atmospheric CO_2 concentration. *Geophysical Research Letters*, *32*(12), L12703. https://doi.org/10.1029/2005gl023209

Haines, S., Crout, R., Bosch, J., Burnett, W., Fredericks, J., Symonds, D., & Thomas, J. (2011). A summary of quality control tests for waves and in situ currents and their effectiveness. In *IEEE/OES 10th Current, Waves and Turbulence Measurements (CWTM)* (pp. 100–106). https://doi.org/10.1109/CWTM.2011.5759534

Heiderich, J., & Todd, R. E. (2020). Along-stream evolution of Gulf Stream volume transport. *Journal of Physical Oceanography*, *50*(8), 2251–2270. https://doi.org/10.1175/jpo-d-19-0303.1

Hellweger, F. L., & Gordon, A. L. (2002). Tracing Amazon river water into the Caribbean Sea. *Journal of Marine Research*, *60*(4), 537–549. https://doi.org/10.1357/002224002762324202

Høydalsvik, F., Mauritzen, C., Orvik, K. A., LaCasce, J. H., Lee, C. M., & Gobat, J. (2013). Transport estimates of the Western branch of the Norwegian Atlantic current from glider surveys. *Deep Sea Research Part I: Oceanographic Research Papers*, *79*, 86–95. https://doi.org/10.1016/j.dsr.2013.05.005

Johns, E., Wilson, W. D., & Molinari, R. L. (1999). Direct observations of velocity and transport in the passages between the intra-Americas Sea and the Atlantic Ocean 1984-1996. *Journal of Geophysical Research*, *104*(C11), 25805–25820. https://doi.org/10.1029/1999jc900235

Johns, W. E., Townsend, T. L., Fratantoni, D. M., & Wilson, W. D. (2002). On the Atlantic inflow to the Caribbean Sea. *Deep Sea Research Part I: Oceanographic Research Papers*, *49*(2), 211–243. https://doi.org/10.1016/s0967-0637(01)00041-3

Johns, W. E., Zantopp, R. J., & Goni, G. J. (2003). Cross-gyre transport by North Brazil current rings. In *Interhemispheric water exchange in the Atlantic Ocean* (Vol. 68, pp. 411–441). Elsevier Oceanography Series. https://doi.org/10.1016/S0422-9894(03)80156-3

Jury, M. R. (2017). Spatial gradients in climatic trends across the southeastern Antilles 1980–2014. *International Journal of Climatology*, *37*(15), 5181–5191. https://doi.org/10.1002/joc.5156
Jury, M. R. (2020). Slowing of Caribbean through-flow. *Deep Sea Research Part II: Topical Studies in Oceanography*, *180*, 104682. https://doi.org/10.1016/j.dsr2.2019.104682
Jury, M. R., & Gouirand, I. (2011). Decadal climate variability in the eastern Caribbean. *Journal of Geophysical Research*, *116*(D21), D00Q03. https://doi.org/10.1029/2010jd015107
Kirchner, K., Rhein, M., Hüttl-Kabus, S., & Böning, C. W. (2009). On the spreading of South Atlantic water into the northern hemisphere. *Journal of Geophysical Research*, *114*(C5), C05019. https://doi.org/10.1029/2008jc005165
Kirchner, K., Rhein, M., Mertens, C., Böning, C. W., & Hüttl, S. (2008). Observed and modeled meridional overturning circulation related flow into the Caribbean. *Journal of Geophysical Research*, *113*(C3), C03028. https://doi.org/10.1029/2007jc004320
Kjerfve, B. (1981). Tides of the Caribbean Sea. *Journal of Geophysical Research*, *86*(C5), 4243–4247. https://doi.org/10.1029/JC086iC05p04243
Lindstrom, E., Gunn, J., Fischer, A., McCurdy, A., & Glover, L. K. (2012). *A framework for ocean observing. By the task team for an integrated framework for sustained ocean observing*. UNESCO. https://doi.org/10.25607/OBP-127
Lobelle, D., Beaulieu, C., Livina, V., Sévellec, F., & Frajka-Williams, E. (2020). Detectability of an AMOC decline in current and projected climate changes. *Geophysical Research Letters*, *47*(20), e2020GL089974. https://doi.org/10.1029/2020gl089974
Locarnini, R. A., Mishonov, A. V., Baranova, O. K., Boyer, T. P., Zweng, M. M., Garcia, H. E., et al. (2018). World Ocean Atlas 2018, volume 1: Temperature. A. Mishonov Technical. In *NOAA Atlas NESDIS 81* (p. 52).
Ma, W., Wang, Y., Wang, S., Zhang, H., Zhang, H., & Gong, Q. (2019). Absolute current estimation and sea-Trial Application of glider-mounted AD2CP. *Journal of Coastal Research*, *35*(6), 1343. https://doi.org/10.2112/jcoastres-d-18-00176.1
Mertens, C., Rhein, M., Walter, M., & Kirchner, K. (2009). Modulation of the inflow into the Caribbean Sea by North Brazil current rings. *Deep Sea Research Part I: Oceanographic Research Papers*, *56*(7), 1057–1076. https://doi.org/10.1016/j.dsr.2009.03.002
Metcalf, W. G. (1976). Caribbean-Atlantic water exchange through the Anegada-Jungfern passage. *Journal of Geophysical Research*, *81*(36), 6401–6409. https://doi.org/10.1029/jc081i036p06401
Miles, T., Seroka, G., Kohut, J., Schofield, O., & Glenn, S. (2015). Glider observations and modeling of sediment transport in Hurricane Sandy. *Journal of Geophysical Research: Oceans*, *120*(3), 1771–1791. https://doi.org/10.1002/2014jc010474
Morrison, J. M., & Nowlin, W. D. (1982). General distribution of water masses within the eastern Caribbean Sea during the winter of 1972 and fall of 1973. *Journal of Geophysical Research*, *87*(C6), 4207. https://doi.org/10.1029/jc087ic06p04207
Nürnberg, D., Riff, T., Bahr, A., Karas, C., Meier, K., & Lippold, J. (2021). Western boundary current in relation to Atlantic Subtropical Gyre dynamics during abrupt glacial climate fluctuations. *Global and Planetary Change*, *201*, 103497. https://doi.org/10.1016/j.gloplacha.2021.103497
Poole, R., & Tomczak, M. (1999). Optimum multiparameter analysis of the water mass structure in the Atlantic Ocean thermocline. *Deep Sea Research Part I: Oceanographic Research Papers*, *46*(11), 1895–1921. https://doi.org/10.1016/s0967-0637(99)00025-4
Praetorius, S. K. (2018). North Atlantic circulation slows down. *Nature*, *556*(7700), 180–181. https://doi.org/10.1038/d41586-018-04086-4
Rahmstorf, S. (2002). Ocean circulation and climate during the past 120,000 years. *Nature*, *419*(6903), 207–214. https://doi.org/10.1038/nature01090
Reißig, S., Nürnberg, D., Bahr, A., Poggemann, D.-W., & Hoffmann, J. (2019). Southward displacement of the North Atlantic subtropical gyre circulation system during North Atlantic cold spells. *Paleoceanography and Paleoclimatology*. https://doi.org/10.1029/2018pa003376
Rhein, M., Kirchner, K., Mertens, C., Steinfeldt, R., Walter, M., & Fleischmann-Wischnath, U. (2005). Transport of South Atlantic water through the passages south of Guadeloupe and across 16N 2000-2004. *Deep Sea Research Part I: Oceanographic Research Papers*, *52*(12), 2234–2249. https://doi.org/10.1016/j.dsr.2005.08.003
Roquet, F., Madec, G., Brodeau, L., & Nycander, J. (2015). Defining a simplified yet realistic equation of state for seawater. *Journal of Physical Oceanography*, *45*(10), 2564–2579. https://doi.org/10.1175/jpo-d-15-0080.1
Rudnick, D. L., Sherman, J. T., & Wu, A. P. (2018). Depth-average velocity from spray underwater gliders. *Journal of Atmospheric and Oceanic Technology*, *35*(8), 1665–1673. https://doi.org/10.1175/jtech-d-17-0200.1
Schmidt, M. W., Spero, H. J., & Lea, D. W. (2004). Links between salinity variation in the Caribbean and North Atlantic thermohaline circulation. *Nature*, *428*(6979), 160–163. https://doi.org/10.1038/nature02346
Schmitz, W. J. (1995). On the interbasin-scale thermohaline circulation. *Reviews of Geophysics*, *33*(2), 151. https://doi.org/10.1029/95rg00879
Schmitz, W. J., & McCartney, M. S. (1993). On the North Atlantic circulation. *Reviews of Geophysics*, *31*(1), 29–49. https://doi.org/10.1029/92rg02583
Schmitz, W. J., & Richardson, P. L. (1991). On the sources of the Florida current. *Deep-Sea Research Part A Oceanographic Research Papers*, *38*, S379–S409. https://doi.org/10.1016/s0198-0149(12)80018-5
Schofield, O., Kohut, J., Aragon, D., Creed, L., Graver, J., Haldeman, C., et al. (2007). Slocum gliders: Robust and ready. *Journal of Field Robotics*, *24*(6), 473–485. https://doi.org/10.1002/rob.20200
Schott, F. A., Fischer, J., & Stramma, L. (1998). Transports and pathways of the upper-layer circulation in the western tropical Atlantic. *Journal of Physical Oceanography*, *28*(10), 1904–1928. https://doi.org/10.1175/1520-0485(1998)028<1904:tapotu>2.0.co;2
Shrikumar, A., Lawrence, R., & Casciotti, K. L. (2021). PYOMPAVersion (0.3). Retrieved 2023, from https://github.com/nitrogenlab/pyompa
Stommel, H. (1989). The Slocum mission. *Oceanography*, *89*(1), 22–25. https://doi.org/10.5670/oceanog.1989.26
Stramma, L., & Schott, F. (1999). The mean flow field of the tropical Atlantic Ocean. *Deep Sea Research Part II: Topical Studies in Oceanography*, *46*(1–2), 279–303. https://doi.org/10.1016/s0967-0645(98)00109-x
Szuts, Z. B., & Meinen, C. S. (2017). Florida current salinity and salinity transport: Mean and decadal changes. *Geophysical Research Letters*, *44*(20), 10495–10503. https://doi.org/10.1002/2017gl074538
Taylor, J. A., & Jonas, A. M. (2008). Maximising data return: Towards a quality control strategy for managing and processing TRDI ADCP data sets from moored instrumentation. *IEEE/OES 9th Working Conference on Current Measurement Technology*, *2008*, 80–88. https://doi.org/10.1109/CCM.2008.4480848
Thornalley, D. J. R., Oppo, D. W., Ortega, P., Robson, J. I., Brierley, C. M., Davis, R., et al. (2018). Anomalously weak Labrador Sea convection and Atlantic overturning during the past 150 years. *Nature*, *556*(7700), 227–230. https://doi.org/10.1038/s41586-018-0007-4
Todd, R. E., Rudnick, D. L., Mazloff, M. R., Davis, R. E., & Cornuelle, B. D. (2011). Poleward flows in the southern California Current System: Glider observations and numerical simulation. *Journal of Geophysical Research*, *116*(C2), C02026. https://doi.org/10.1029/2010jc006536
Todd, R. E., Rudnick, D. L., Sherman, J. T., Owens, W. B., & George, L. (2017). Absolute velocity estimates from autonomous underwater gliders equipped with Doppler current profilers. *Journal of Atmospheric and Oceanic Technology*, *34*(2), 309–333. https://doi.org/10.1175/jtech-d-16-0156.1

Tomczak, M., & Large, D. G. B. (1989). Optimum multiparameter analysis of mixing in the thermocline of the eastern Indian Ocean. *Journal of Geophysical Research*, *94*(C11), 16141. https://doi.org/10.1029/jc094ic11p16141

Tuchen, F. P., Brandt, P., Lübbecke, J. F., & Hummels, R. (2022). Transports and pathways of the tropical AMOC return flow from Argo data and shipboard velocity measurements. *Journal of Geophysical Research: Oceans*, *127*(2), e2021JC018115. https://doi.org/10.1029/2021jc018115

Visbeck, M. (2002). Deep velocity profiling using lowered acoustic Doppler current profilers: Bottom track and inverse solutions. *Journal of Atmospheric and Oceanic Technology*, *19*(5), 794–807. https://doi.org/10.1175/1520-0426(2002)019<0794:dvpula>2.0.co;2

Wajsowicz, R. C. (2002). A modified Sverdrup model of the Atlantic and Caribbean circulation. *Journal of Physical Oceanography*, *32*(3), 973–993. https://doi.org/10.1175/1520-0485(2002)032<0973:amsmot>2.0.co;2

Wilson, W. D., & Johns, W. E. (1997). Velocity structure and transport in the Windward Islands passages. *Deep Sea Research Part I: Oceanographic Research Papers*, *44*(3), 487–520. https://doi.org/10.1016/s0967-0637(96)00113-6

Worthington, L. V. (1958). The 18 water in the Sargasso Sea. *Deep-Sea Research*, *5*(2–4), 297–305. https://doi.org/10.1016/0146-6313(58)90026-1

Zhang, D., Mcphaden, M. J., & Johns, W. E. (2003). Observational evidence for flow between the subtropical and tropical Atlantic: The Atlantic subtropical cells*. *Journal of Physical Oceanography*, *33*(8), 1783–1797. https://doi.org/10.1175/2408.1

Zweng, M. M., Reagan, J. R., Seidov, D., Boyer, T. P., Locarnini, R. A., Garcia, H. E., et al. (2018). World Ocean Atlas 2018, volume 2: Salinity. A. Mishonov Technical. In *NOAA Atlas NESDIS 82* (p. 50).